

## SUPPORTING INFORMATION

# **Sustainable synthesis of amino acids by catalytic fixation of molecular dinitrogen and carbon dioxide**

Manuel Rivas<sup>1</sup>, Luís J. del Valle<sup>1,2</sup>, Pau Turon<sup>1,3\*</sup>, Carlos Alemán<sup>1,2\*</sup>, and Jordi  
Puiggali<sup>1,2\*</sup>

<sup>1</sup> Departament d'Enginyeria Química, EEBE, Universitat Politècnica de Catalunya, C/ Eduard  
Maristany, 10-14, 08019, Barcelona, Spain.

<sup>2</sup> Barcelona Research Center for Multiscale Science and Engineering, Universitat Politècnica  
de Catalunya, C/ Eduard Maristany, 10-14, Ed. C, 08019, Barcelona, Spain

<sup>3</sup> B. Braun Surgical, S.A. Carretera de Terrasa 121, 08191 Rubí (Barcelona), Spain

## **Materials and Methods**

### **Materials**

Diammonium hydrogen phosphate  $[(\text{NH}_4)_2\text{HPO}_4]$ ; purity  $\geq 99.0\%$ , ammonium hydroxide solution 30% ( $\text{NH}_4\text{OH}$ ; purity: 28-30% w/w), calcium nitrate ( $\text{Ca}(\text{NO}_3)_2$ ), zirconyl chloride (ZC:  $\text{ZrOCl}_2 \cdot 8\text{H}_2\text{O}$ ), amino tris(methylene phosphonic acid (ATMP), 2,2-dihydroxyindane-1,3-dione (ninhydrin), Glycine (aminoacetic acid), L-Alanine ((S)-2-aminopropionic acid) and D-Alanine ((R)-2-aminopropionic acid) were purchased from Sigma-Aldrich. Pristine sodium montmorillonite (Nanofil 757, N757), denoted silicate in the main text, was purchased from Süd-Chemie (Germany) and layered mica (LM), denoted aluminosilicate, from Agar Scientific.  $\text{N}_2$ ,  $\text{CH}_4$  and  $\text{CO}_2$  gases with a purity of  $> 99.995\%$  were purchased from Messer. Solvents (ethanol and acetone) were purchased from Scharlab. All experiments were performed with milli-Q water.

### **Synthesis of amorphous (aHAp) and crystalline hydroxyapatite (cHAp)**

15 mL of 0.5 M  $(\text{NH}_4)_2\text{HPO}_4$  in de-ionized water (pH adjusted to 11 with an ammonium hydroxide 30 w/w-% solution) were added drop-wise (rate of  $2 \text{ mL} \cdot \text{min}^{-1}$ ) and under agitation (400 rpm) to 25 mL of 0.5 M  $\text{Ca}(\text{NO}_3)_2$  in ethanol. After that, the reaction mixture was stirred 1 h by agitation (400 rpm) at room temperature. The suspension was aged for 24 h at  $37^\circ \text{C}$  to achieve aHAP, whereas a hydrothermal treatment (200 bar at  $150^\circ \text{C}$  for 24 h) was subsequently applied to obtain cHAp. The precipitates were separated by centrifugation and washed sequentially with milli-Q water and a 60/40 v/v mixture of ethanol-water (twice). A white powder with the theoretical Ca/P ratio of 1.67 was recovered after freeze-drying.

### **Sintering process**

aHAp, cHAp, and montmorillonite and mica powders were sintered by firstly heating them in a laboratory furnace (Carbolite ELF11/6B/301) at 1000 °C during 2 h at an air atmosphere and finally uniaxially pressed at 620 MPa for 10 min. Discs of 10 mm of diameter, 1.7 mm of thickness and sufficient mechanical consistence (s-aHAp, s-cHAp, s-Nanofil 757 and s-LM) were finally obtained.

### **Thermally and electrically stimulated polarization process**

In order to get thermally and electrically stimulated minerals, discs of s-cHAp, s-aHAp, s-Nanofil 757 or s-LM were sandwiched between stainless steel (AISI 304) plates, heated in the furnace to 1000 °C in air and, simultaneously, polarized for 1 h under application of a constant DC voltage of 500 V. Subsequently, samples were cooled to room temperature, maintaining the DC voltage, the resultant polarized systems being denoted p-aHAp, p-cHAp, p-N757 and p-LM, respectively. These conditions were defined from preliminary assays with s-cHAp discs using DC voltages that ranged from 250 to 2000 V. The best results, in terms of both mechanical consistence and maximum adsorption capacity of phosphates and phosphonates (not shown), were obtained at 500 V.

### **Characterization of polarized hydroxyapatite (p-cHAp)**

The electrochemical behavior was determined by cyclic voltammetry (CV) using an Autolab PGSTAT302N equipped with the ECD module (Ecochimie, The Netherlands) with a three-electrode cell under a nitrogen atmosphere (99.995% in purity) at room temperature. A 0.1 M phosphate buffer saline solution (PBS; pH = 7.2 adjusted with NaOH) was used as the

electrolyte in the three-electrode cell. The working compartment was filled with 30 mL of the electrolyte solution. Steel AISI 316 sheets of  $1 \times 1.5 \text{ cm}^2$  (thickness 0.1 cm) were used as both the working and the counter electrodes, and an Ag|AgCl electrode was used as the reference electrode which contained a KCl saturated aqueous solution (offset potential versus the standard hydrogen electrode,  $E^0 = 0.222 \text{ V}$  at  $25 \text{ }^\circ\text{C}$ ). All potentials given in this report are referenced to this electrode. Polarized HAp (p-HAp) discs, prepared as described above, were fixed on the working electrode using a two-side adhesive carbon layer. The initial and final potentials were  $-0.40 \text{ V}$ , whereas a reversal potential of  $0.80 \text{ V}$  was considered. The scan rate was  $50 \text{ mV/s}$ .

The crystallinity and structure was studied by wide angle X-ray diffraction (WAXD). Patterns were acquired using a Bruker D8 Advance model with  $\text{Cu K}_\alpha$  radiation ( $\lambda = 0.1542 \text{ nm}$ ) and geometry of Bragg-Brentano, theta-2 theta. A one-dimensional Lynx Eye detector was employed. Samples were run at  $40 \text{ kV}$  and  $40 \text{ mA}$ , with a 2-theta range of  $10\text{-}60$ , measurement steps of  $0.02^\circ$ , and time/step of  $2\text{-}8 \text{ s}$ . Diffraction profiles were processed using PeakFit v4 software (Jandel Scientific Software) and the graphical representation performed with OriginPro v8 software (OriginLab Corporation, USA). The crystallite size ( $L$ ), in the direction perpendicular to the (211) planes, was derived from X-ray diffraction profiles considering the (211) peak width and line broadening measurement using the Scherrer equation:<sup>S1</sup>

$$L = \frac{0.9\lambda}{\beta \cos \theta} \quad (1)$$

where  $\lambda$  is the wavelength ( $\text{CuK}_\alpha$ ),  $\beta$  is the full width at half maximum height of the (211) peak,  $\theta$  is the diffraction angle and 0.9 is a shape factor.

The crystallinity ( $\chi_c$ ) was obtained using the following expression:<sup>S2</sup>

$$\chi_c = 1 - \frac{V_{112/300}}{I_{300}} \quad (2)$$

where  $I_{300}$  is the intensity of the (300) reflection and  $V_{112/300}$  is the intensity of the hollow between the (112) and (300) reflections, which disappears in non-crystalline samples.

Cyclic voltammograms recorded in PBS for cHAp *as prepared*, *sintered* and *polarized* are compared in Figure S1a. The electrochemical activity of *as prepared* cHAp is higher than that of steel AISI 316, which was used as a control. However, the electrochemical activity, which indicates the ability to exchange charge reversibly, increases considerably upon application of sintering and thermally and electrically stimulated polarization treatments (*i.e.* 41% and 159%, respectively). In the case of p-cHAp, such effect is accompanied by a significant enhancement of the anodic current intensity at the reversal potential. This behavior has been attributed to the structural changes caused by the thermally and electrically stimulated polarization treatment, which facilitates the diffusion of ions through the inorganic matrix and, therefore, the electrochemical response upon oxidation-reduction processes. These structural changes are reflected in Table S1. The  $\chi_c$  of p-cHAp and *as prepared* cHAp are  $0.77 \pm 0.03$  and  $0.41 \pm 0.02$ , respectively, while the crystallite size of p-cHAp is around 40% larger than that of *as prepared* cHAp. The variation of  $\chi_c$  and  $L$  has been related with the formation of OH<sup>-</sup> defects.

On the other hand, cyclic voltammograms of polarized samples obtained using p-cHAp and p-aHAp are compared in Figure S1b. As can be seen, the electrochemical activity of p-aHAp is very noteworthy, even though lower than that of p-cHAp. This reduction has been attributed to partial decomposition suffered by aHAp during the sintering process, which led to the formation of  $\beta$ -tricalcium phosphate ( $\beta$ -TCP:  $\beta$ -Ca<sub>3</sub>(PO<sub>4</sub>)<sub>2</sub>). Thermal decomposition of aHAp at temperatures close to 1000 °C has also been reported by different authors.<sup>S3,S4</sup>

### **Deposition of phosphonate and zirconyl chloride layers**

A 3-layered system consisting in the successive deposition of ATMP, ZC and ATMP layers (Phos-ZC-Phos) onto a mineral substrate (*i.e.* s-cHAp, s-aHAp, s-Nanofil 757 or s-LM before and after being submitted to the thermally stimulated polarization process) was obtained by immersion in the corresponding aqueous solutions at room temperature for 5 h. Concentrations of ATMP solutions to obtain the first and third ATMP layers were 5 mM and 1.25 mM, respectively, whereas the concentration of ZC was varied from 1 mM to 10 mM. After each immersion the samples were dried at 37 °C for 3 h. For the sake of completeness, 2-layered and 1-layered systems (*i.e.* Phos-ZC, ZC-Phos, Phos and ZC) were also considered.

### **Synthesis of amino acids**

A high pressure stainless steel reactor was designed *ad hoc* and employed to perform the synthesis of amino acids (AAs). The designed reactor, which is schematized in Figure S1, was dotted with a manometer, an electric heater with a thermocouple and an external temperature controller. The reactor was also characterized by an inert reaction chamber coated with a perfluorinated polymer (120 mL) where both the catalyst and water were incorporated. The reactor was equipped with three independent inlet valves for N<sub>2</sub>, CH<sub>4</sub>, CO<sub>2</sub> and an outlet valve to recover the gaseous reaction products. A UV lamp (GPH265T5L/4, 253.7 nm) was also placed in the middle of the reactor to irradiate the catalyst directly, the lamp being protected by a UV transparent quartz tube. All surfaces were coated with a thin film of a perfluorinated polymer in order to avoid any contact between the reaction medium and the reactor surfaces, in this way discarding other catalyst effects.

Regarding temperature range, the reactions were performed within 75-105 °C for reaction times ranging from 2 to 96 h. Catalyst samples weighed approximately 150 mg and 0.5 mL of de-ionized liquid water were initially incorporated into the reaction chamber, except for assessing the water effect. The chamber was extensively purged with the first selected gas in order to eliminate the initial air content. Each selected gas was introduced to increase the reaction chamber pressure (measured at room temperature) to the target pressure (*i.e.* 1 or 6 bar).

As mentioned in the previous sub-section, the concentration of ZC was varied from 1 mM to 10 mM for the preparation of Phos-ZC-Phos trilayer. However, the influence of the content of ZC on the yield of Gly and Ala is very small. This is shown in Figure S2, which displays the variation of the Gly/Phos and Ala/Phos ratios using p-cHAp/Phos-ZC-Phos catalytic systems in which the ZC layer was deposited from concentrations ranging from 1 to 10 mM. According to these results, all the results displayed in this work, including the main text, correspond to ZC layer deposited from a 5 mM solution (unless another concentration is explicitly indicated).

## **Measurements**

Synthesis of AAs was routinely verified by the ninhydrin (2,2-dihydroxyindane-1,3-dione) detection test for primary amines.<sup>S5</sup>. To this end 0.5 mg of the solid recovered after reaction was immersed in a tube containing 0.2 w/v-% solution of ninhydrin in acetone and subsequently heated to 75 °C in an oven. The development of purple coloured solutions indicated the formation of the 2-(1,3-dioxindan-2-yl)iminoindane-1,3-dione chromophore. No yellow-orange coloured solutions were observed characteristic of the Schiff base generated by reaction with secondary amines.

All NMR spectra were acquired with a Bruker Avance III-400 spectrometer operating at frequencies of 400.1 MHz, 100.6, and 161.9 for  $^1\text{H}$ ,  $^{13}\text{C}$  and  $^{31}\text{P}$ , respectively. Chemical shifts were calibrated using tetramethylsilane ( $^1\text{H}$  and  $^{13}\text{C}$ ) and  $\text{H}_3\text{PO}_4$  ( $^{31}\text{P}$ ) as internal standards. Sixty-four, one thousand and two hundred fifty-six scans were recorded for  $^1\text{H}$ ,  $^{13}\text{C}$  and  $^{31}\text{P}$  NMR, respectively. In order to remove the AAs from the catalyst, samples were dissolved in deuterated water containing 100 mM of HCl and 50 mM of NaCl.

$^1\text{H}$  NMR spectra were analyzed for samples recovered after reaction times ranging from 2 to 96 h to detect the Gly/Phos and Ala/Phos ratios through the areas of signals corresponding to  $\text{CH}_2$  protons at 3.65 ppm (Gly) and 3.79-3.76 ppm (Phos) and the  $\text{CH}_3$  protons at 1.54-1.52 ppm (Ala).

$$\text{Gly/Phos} = (3 \times A_{3.65}) / A_{3.79-376} \quad (1)$$

$$\text{Ala/Phos} = (2 \times A_{1.54-1.52}) / A_{3.79-376} \quad (2)$$

$$\text{Gly/Ala} = (1.5 \times A_{3.65}) / A_{1.54-1.52} \quad (3)$$

X-ray photoelectron spectroscopy (XPS) analyses were performed in a SPECS system equipped with a high-intensity twin-anode X-ray source XR50 of Mg/Al (1253 eV/1487 eV) operating at 150 W, placed perpendicular to the analyzer axis, and using a Phoibos 150 MCD-9 XP detector. The X-ray spot size was 650  $\mu\text{m}$ . The pass energy was set to 25 and 0.1 eV for the survey and the narrow scans, respectively. Charge compensation was achieved with a combination of electron and argon ion flood guns. The energy and emission current of the electrons were 4 eV and 0.35 mA, respectively. For the argon gun, the energy and the emission current were 0 eV and 0.1 mA, respectively. The spectra were recorded at a pressure below  $6 \times 10^{-9}$  mbar. These standard conditions of charge compensation resulted in a negative but

perfectly uniform static charge. The C1s peak was used as an internal reference with a binding energy of 284.8 eV. High-resolution XPS spectra were acquired by the Gaussian–Lorentzian curve fitting after s-shape background subtraction. The surface composition was determined using the manufacturer's sensitivity factors.

Scanning electron microscopy (SEM) studies were carried out using a Focused Ion Beam Zeiss Neon40 microscope operating at 5 kV, equipped with an energy dispersive X-ray (EDX) spectroscopy system. Samples were deposited on a silicon disc mounted with silver paint on pin stubs of aluminum, and sputter-coated with a thin layer of carbon to prevent sample charging problems.

Infrared absorption spectra were recorded with a Fourier Transform FTIR 4100 Jasco spectrometer in the 1800-700  $\text{cm}^{-1}$  range. A Specac model MKII Golden Gate attenuated total reflection (ATR) equipment with a heating Diamond ATR Top-Plate was used.

X-ray powder diffraction patterns were recorded in the beamline BL11-NCD at ALBA synchrotron (Cerdanyola del Vallés, Barcelona, Spain) using a wavelength of 0.100 nm and an WAXS LX255-HS detector from Rayonix, which was calibrated with diffractions of standard of a  $\text{Cr}_2\text{O}_3$  sample.

The separation of the synthesized AAs was performed by HPLC on a Agilent serie 1200 chromatograph using a Chirobiotic T (250 × 4.6 mm) column with a particle size of 5  $\mu\text{m}$ . The mobile phase consisted of methanol:water (60:40 v/v) mixture. The flow rate was set at 1 mL/min and the volume of injected samples was 20  $\mu\text{L}$ . The column temperature was maintained at 25°C. Chromatograms were recorded at three wavelengths (205.4, 210.4 and 215.4 nm), but 210.4 nm was used for quantification purposes. Retention times of each AA were identified by comparing with the corresponding standard: 5.168 min (L-Ala), 5.781 min

(Gly) and 7.463 min (D-Ala). Injected samples were obtained by extracting the AA from the catalyst after reaction (10 mg) using a mixture of 1 mL of methanol:water (60:40 v/v) by shaking during 5 min. After 30 min of sedimentation, the supernatant was filtered using a PTFE 0.2  $\mu\text{m}$  filter and finally, 20  $\mu\text{L}$  of such a filtrate were injected into the HPLC equipment. Analysis of volatile organic compounds has been carried out by employing an Agilent GC 7890B gas chromatograph equipped with an Agilent MSD 5975C mass selective detector. Samples were previously adsorbed in a multi-sorbent bed (Carbotrap, Carbopack X, Carboxen 569). Formaldehyde was determined by using an Empower Alliance 2795 high resolution liquid chromatograph dotted with a Waters UV/Vis detector and Empower Waters software. A Zorbax Eclipse Plus C18 column was employed and the separation was performed using a water/acetonitrile (45/55) mixture as eluent under a flow rate of 1.2 mL/min. Samples were adsorbed in 2,4-dinitrophenylhydrazine-coated silica gel cartridge having a built-in ozone scrubber.

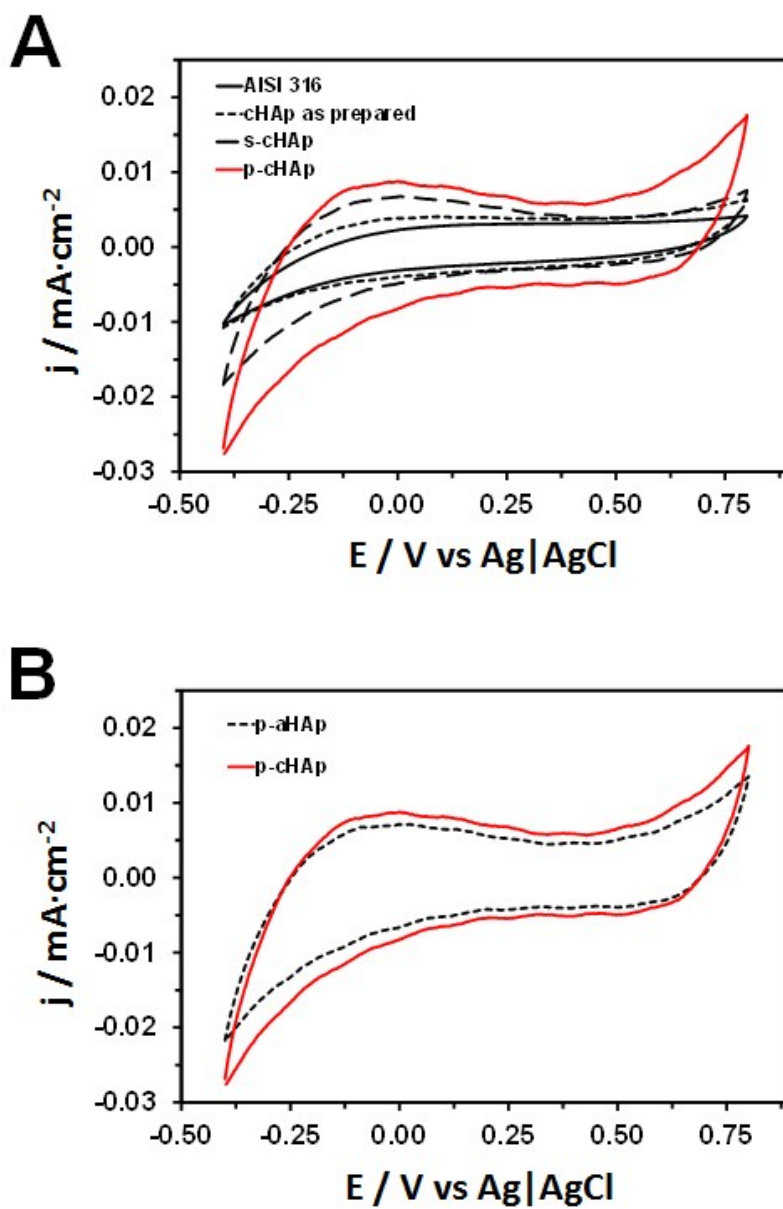


**Figure S1.** Control cyclic voltammograms comparing the electrochemical activity of: (A) cHAp *as prepared*, *sintered* (s-cHAp) and *polarized* (p-cHAp); and (B) p-aHAp and p-cHAp.

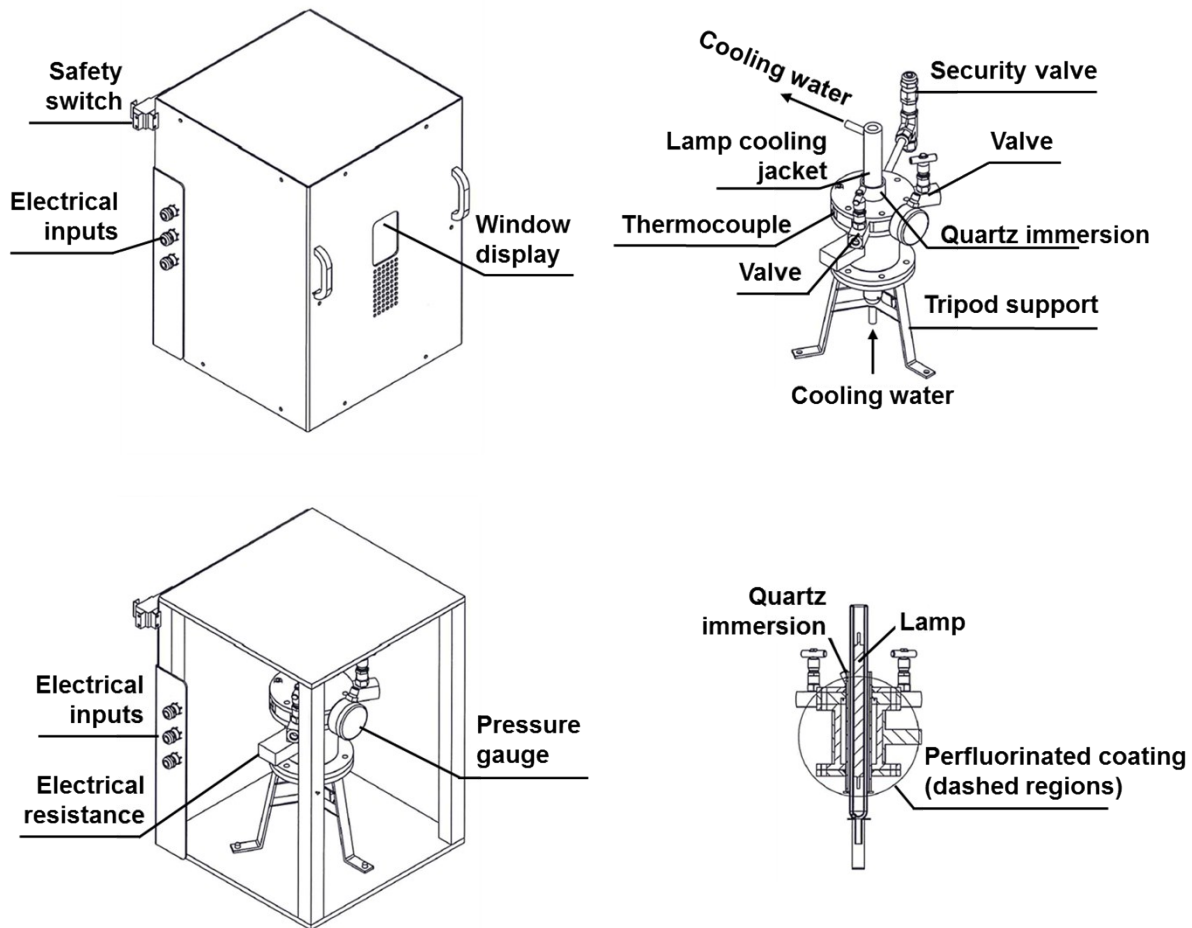


**Figure S2.** Details of the reactor designed to synthesize AAs.

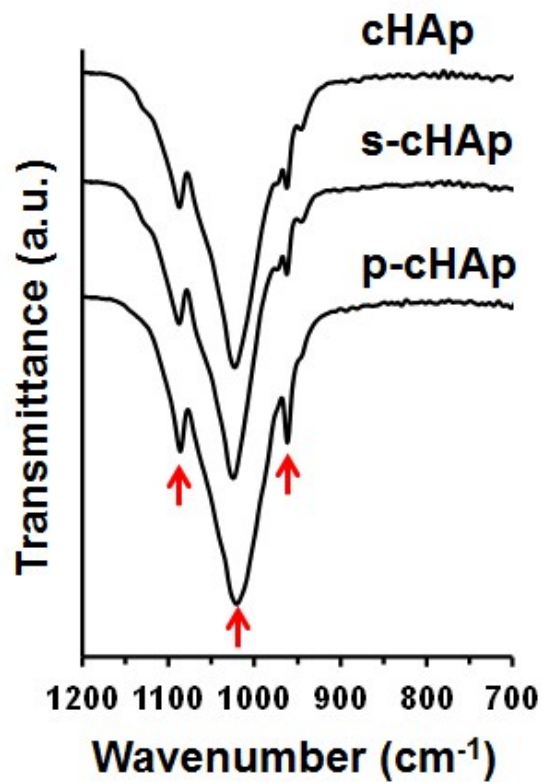


**Figure S3.** FTIR spectra of cHAp *as prepared*, *sintered* (s-cHAp) and *polarized* (p-cHAp). The region comprised between 950 and 1200 cm<sup>-1</sup> displays typical PO<sub>4</sub><sup>3-</sup> bands. The spectra of cHAp, s-cHAp and p-cHAp show characteristic vibrational modes of PO<sub>4</sub><sup>3-</sup> at  $\nu_1=962$  cm<sup>-1</sup> and  $\nu_3=1016, 1087$  cm<sup>-1</sup>.

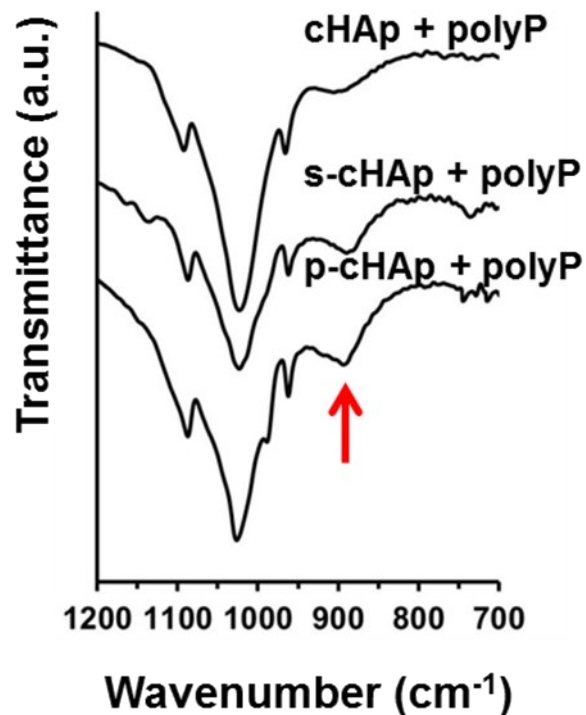


**Figure S4.** FTIR spectra of cHAp as *prepared*, *sintered* (s-cHAp) and *polarized* (p-cHAp). incubated in presence of triphosphate (200 mM) at pH 7. The red arrow indicates the position of the band used to identify the adsorption of triphosphate (PolyP). The weak shoulder identified around 890  $\text{cm}^{-1}$  for cHAp, which corresponds to the P–O–P asymmetric stretching, transforms into a well-defined adsorption band for s-cHAp and, especially, p-cHAp. This feature reflects that the application of thermal and thermally and electrically stimulated polarization processes enhance significantly the ability of cHAp to adsorb polyphosphates. Based on the FTIR spectra presented in Figures S3 and S4, the ability of cHAp samples to adsorb triphosphate was estimated using the ratio of integrated area of the peak at 1016  $\text{cm}^{-1}$  (belonging to the mineral) and the integrated area of the peak at 890  $\text{cm}^{-1}$  (belonging to polyP). Results indicated that the adsorption of polyP onto cHAp was 2.0 and 2.6 times lower than onto s-cHAp and p-cHAp, respectively. These results prove that properties of p-cHAp are clearly unique with respect to cHAp and s-cHAp.

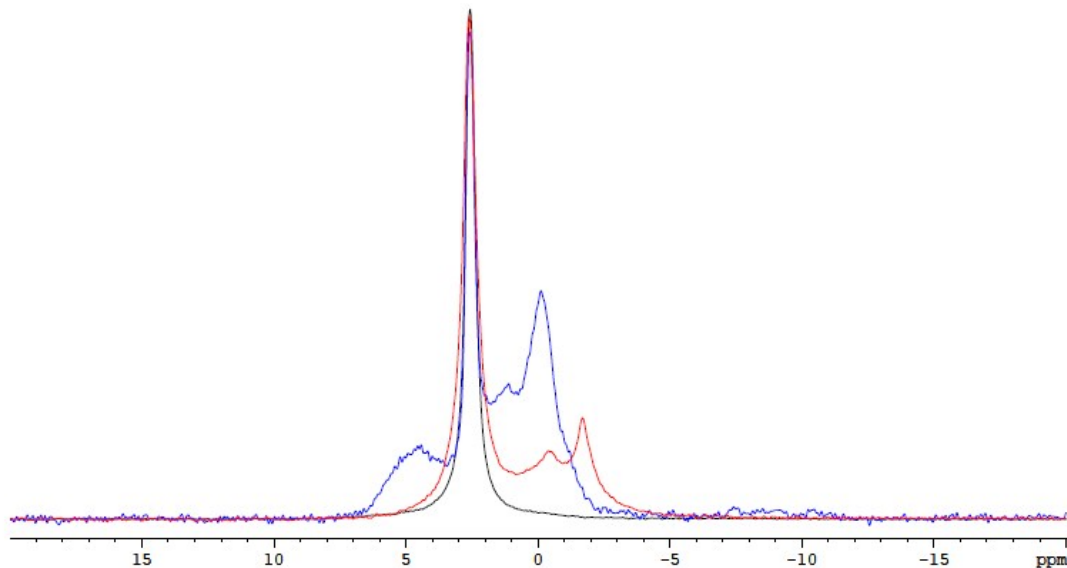


**Figure S5.** Solid state  $^{31}\text{P}$  NMR spectra of cHAp *as prepared* (in blue), *sintered* (s-cHAp; in red) and *polarized* (p-cHAp; in black). The main resonance peak, present in cHAp, s-cHAp and p-cHAp, at 2.9 ppm corresponds to bulk phosphate groups  $\text{PO}_4^{3-}$  of hydroxyapatites.<sup>S7</sup> Note that, compared to cHAp, the band width of s-cHAp and, particularly, p-cHAp samples are narrower, which is consistent with the higher crystallinity of the substrate (Crystallinity (%): cHAp= 42.67; s-cHAp=64.70; p-cHAp=75.50). The broad signals at approximately [-1, 0] ppm and a shoulder at [0,1] ppm, present in cHAp and s-cHAp, were usually assigned to the protonated surfaces phosphate groups arising from the disordered near surface layer.<sup>S8</sup> Indeed, hydroxyapatite particles are typically described as an ordered hydroxyapatite core surrounded by a disordered non-apatitic surface layer.<sup>S9</sup> The shoulder at 4-6 ppm, which is present in s-cHAp, is also due to the surface  $\text{HPO}_4^{2-}$  ions, when its amount in the surface layer is greater than a certain threshold.<sup>S10</sup> This increase in surface of  $\text{HPO}_4^{2-}$  ions in s-cHAp is caused by the more disordered surface layer due to the thermal process applied in s-cHAp particle treatment. The more unusual part is the only peak of typical bulk phosphate groups  $\text{PO}_4^{3-}$  of hydroxyapatites present in p-cHAp. *p-cHAp* particles treatment consists of applying a constant DC electric field of 500 V, heating simultaneously at 1000 ° C for 2 h. This thermally and electrically stimulated polarization process was found to exert different effects on the hydroxyapatite surface properties.<sup>S11</sup> The hydroxyapatite surface undergoes variations due to changes in the position of  $\text{OH}^-$  ions.<sup>S12</sup> Accordingly, the fingerprint of the surface  $\text{OH}^-$  ions

leaving from the columns due to the thermally and electrically stimulated polarization process in p-CHAp is the disappearance of the surface  $\text{HPO}_4^{2-}$  ions and the formation of holes in the valence band ( $h^+$ ) for charge neutralization.

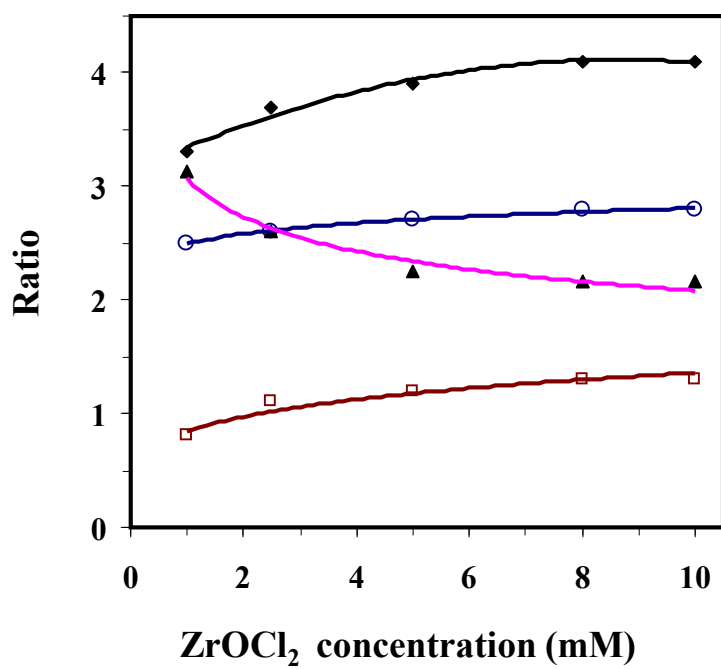


**Figure S6.** Variation of Gly/Phos (○), Ala/Phos (□), (Gly+Ala)/Phos (◆) and Gly/Ala (▲) ratios for reactions performed at 95 °C, 24 h and using the p-cHAp/Phos-ZC-Phos system versus the concentration of ZC solutions used to prepare the central ZC layer (see Figure 1a).

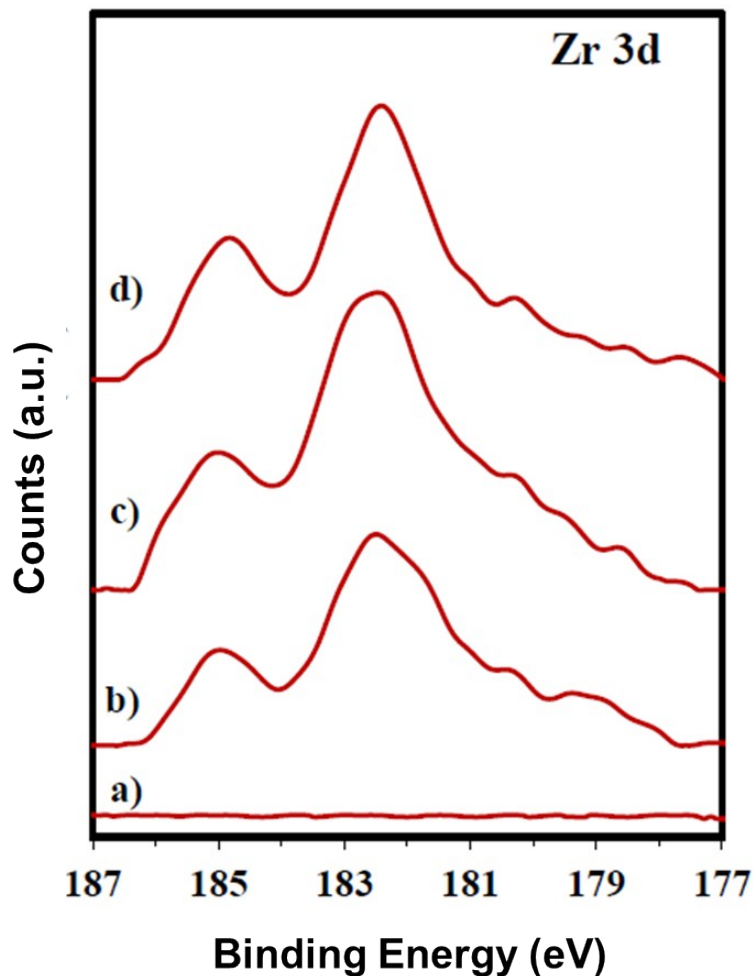


**Figure S7.** Zr 3d high resolution XPS spectra for (a) p-cHAp, (b) p-cHAp/Phos-ZC-Phos, and (c) p-cHAp/Phos-ZC-Phos after negative reaction (*i.e.* without exposure to UV radiation) and (d) p-cHAp/Phos-ZC-Phos after positive reaction (24 h at 95 °C).

The Zr signals appeared as a resolved spin doublet at binding energies of 182.6 and 185.0 eV, which correspond to the 3d<sub>5/2</sub> and 3d<sub>3/2</sub>, respectively.<sup>S5</sup> The measured Zr content was in the 1.26-1.29% interval for all samples having the Phos-ZC-Phos trilayer prepared using a 5 mM ZC solution, this percentage being independent of the progress of the reaction.

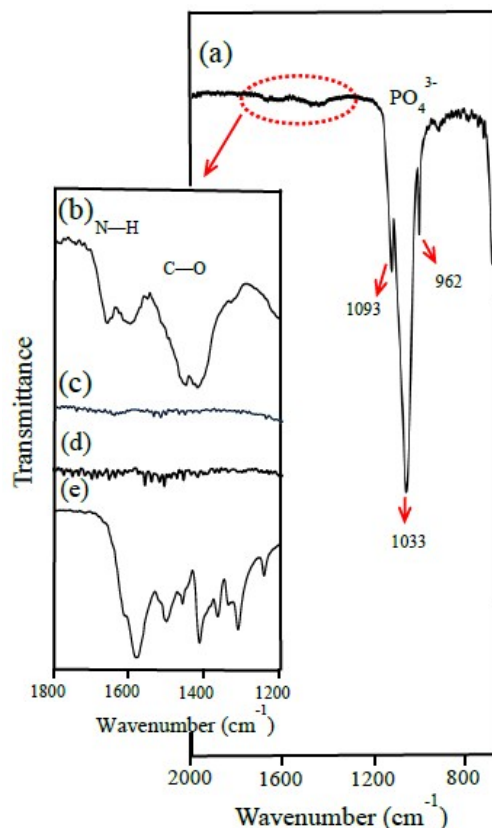


**Figure S8.** (a) FTIR spectra of the sample after reaction for 24 h at 95 °C. Insets compare the 1800-1200  $\text{cm}^{-1}$  region for the above sample (b) after and (c) before reaction, (d) an unsuccessful reaction because of the lack of sustained exposure of the system to the UV radiation, and (e) a mixture of Gly and Ala (2:1 weight ratio).

Despite the low sensitivity of the technique, the successfully formed AAs are identified by the broad and low-intensity bands at the 1600-1400  $\text{cm}^{-1}$  region. It is worth noting that this region is completely flat in the spectra of samples before reaction and also for samples coming from a negative ninhydrin test (e.g. spectrum (c) for samples without UV radiation). On the contrary, AAs such as Gly and Ala have the most intense absorptions in this region (b). Obviously, FTIR spectra showed in all samples the characteristic peaks of HAp and specifically the three intense bands at 1093, 1033 and 962  $\text{cm}^{-1}$  associated with the characteristic vibrational modes of  $\text{PO}_4^{3-}$ .

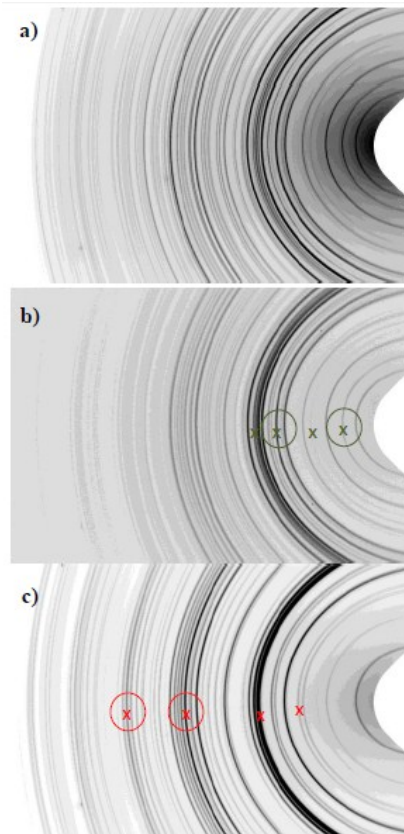


**Figure S9.** X-ray diffraction patterns corresponding to (a) p-cHAp and the p-cHAp/Phos-ZC-Phos system (b) before and (c) after successful reaction for 24 h at 95 °C. Gray crosses in b) point out the characteristic X-ray diffraction reflections of the catalytic system, which disappear after reaction, while red crosses in c) point out new reflections that can be observed after successful reaction. Circled symbols indicate the reflections that changed more drastically during reaction.

Deposition of the 3-layer onto p-cHAp did not cause a significant changes in the X-ray diffraction pattern (a) and (b), whereas remarkable changes can be observed after chemical reaction (b) and (c). These correspond to the disappearance of some reflections (*i.e.* 0.648, 0.406, 0.321 and 0.282 nm) and the appearance /intensification of some reflections (*i.e.* 0.391, 0.282, 0.184 and 0.146 nm). It is clear that reaction gave rise to a slight transformation of the previous structure as reflected by the development of new crystals (Figure 3D). However, characteristic peaks of Ala and Gly were not clearly detected due to overlapping with reflections of catalysts, the development of different crystalline structures for the adsorbed AA, and the low amount of formed crystals.

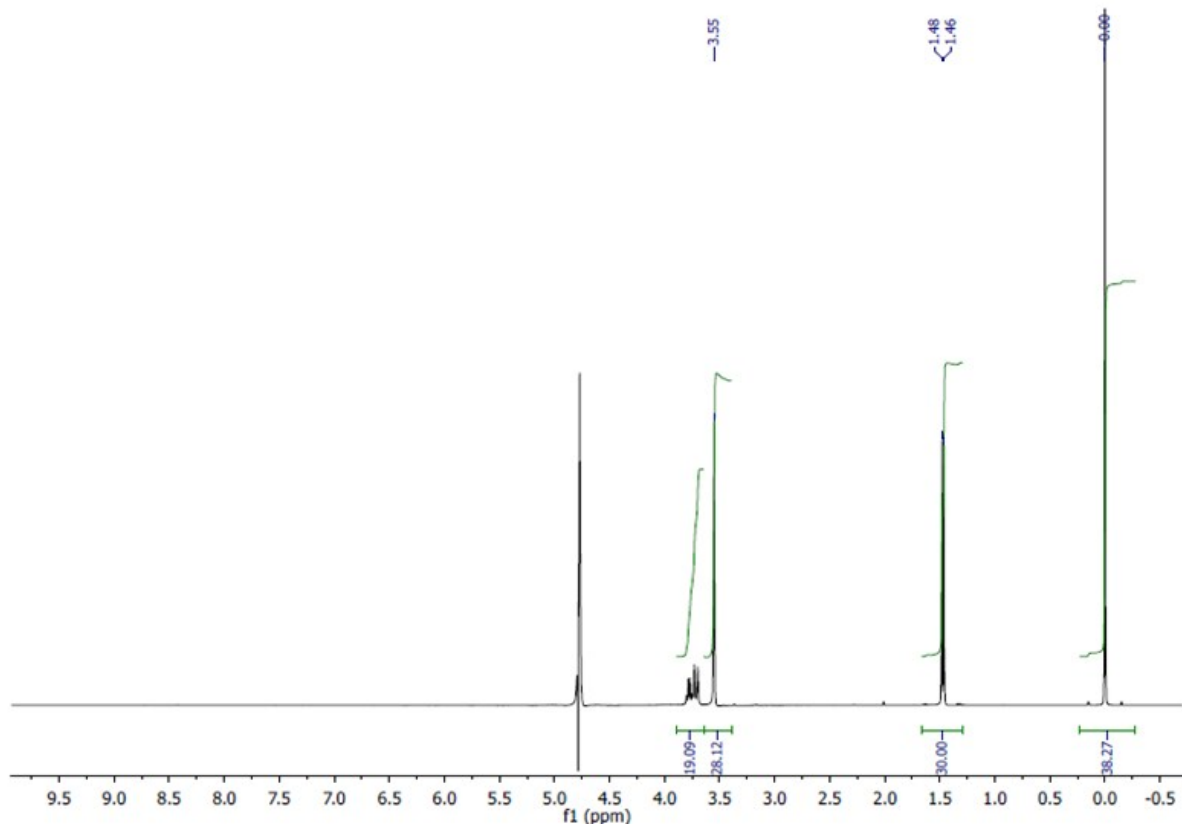


**Figure S10.** <sup>1</sup>H-NMR spectra of samples obtained after reaction (95 °C and 24 h) using a chamber pressure of 6 bar (*i.e.* 2 bar of each feeding reaction gas). The spectrum corresponds to the solution obtained after extraction of the AAs from the catalyst by dissolving the sample in deuterated water containing 100 mM of HCl and 50 mM of NaCl. Gly and Ala peaks are practically identical to those displayed in Figure 2 (*i.e.* using a chamber pressure of 1 bar – 0.33 bar of each feeding reaction gas).

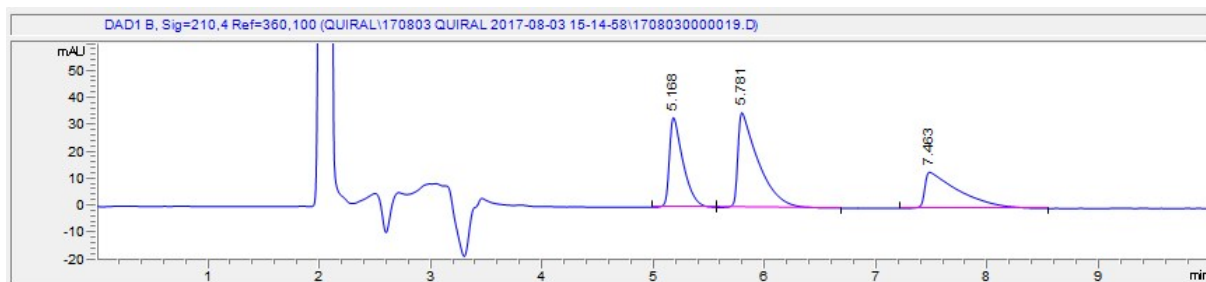


**Figure S11.** Representative HPLC chromatogram ( $\lambda=210.4$  nm) of a sample extracted from the catalyst after reaction shows the separation of Gly (5.781 min), L-Ala (5.168 min) and D-Ala (7.463 min). A racemic D-Ala:L-Ala mixture was obtained.

**Table S1.** Structural parameters of cHAp, aHAp as prepared and after applying the thermally and electrically stimulated polarization treatment: crystallinity ( $\chi_c$ ) and length of the crystallites ( $L$ ).

<b>Sample</b>	<b><math>\chi_c</math> (%)</b>	<b><math>L</math> (nm)</b>
As prepared cHAp	0.41±0.02	61±2
p-cHAp	0.77±0.03	42±3
As prepared aHAp	0.09±0.01	10±1
p-aHAp	0.69±0.03	52±3

**Table S2.** Atomic percent composition (Ca, P, O, C, N and Zr) of p-cHAP, p-cHAP/Phos-ZC-Phos, p-cHAP/Phos-ZC-Phos after negative reaction (*i.e.* without exposure to UV radiation), and p-cHAp/Phos-ZC-Phos after positive reaction (24 h at 95 °C). Reactions were performed at 6 atm.

	<b>Ca</b>	<b>P</b>	<b>O</b>	<b>C</b>	<b>N</b>	<b>Zr</b>
p-cHAp	38.35	17.78	41.96	1.20	0.70	0.01
p-cHAp/Phos-ZC-Phos	34.79	16.21	42.46	1.73	3.12	1.69
p-cHAp/Phos-ZC-Phos (after negative reaction) <sup>a</sup>	25.43	11.86	44.78	5.45	10.72	1.76
p-cHAp/Phos-ZC-Phos (after positive reaction) <sup>b</sup>	22.87	10.46	44.69	7.87	12.43	1.68

<sup>a</sup> Without exposure to UV radiation. <sup>b</sup> 24 h at 95 °C.

**Table S3.** Atomic percent composition (Ca, P, O, C, N and Zr) of p-cHAp, p-cHAp/Phos and HAp/ZC before and after remain in a N<sub>2</sub> atmosphere. As it can be seen, the percentage of N increases considerably when N<sub>2</sub> is in contact with p-cHAp (71% of increment) and, especially, p-cHAp/Phos (261% of increment) indicating that the p-cHAp substrate and the ATMP layers are the catalyst components associated with the first step of the N<sub>2</sub> fixation (*i.e.* adsorption of the gas from the atmosphere). Besides, the increment of the percentage of N for p-cHAp/ZC (62%) is similar to that obtained for p-cHAp, indicating that the role of the ZC layer in the N<sub>2</sub> adsorption is null.

Experiments were performed according to this protocol: i) heating of the sample until 400 °C with an Ar flux during 30 min; ii) cooling down to 90 °C; and ii) generation of a N<sub>2</sub> atmosphere applying a nitrogen flux of 5 mL/min diluted in an Ar flux of 45 mL/min during 30 min.

	<b>Ca</b>	<b>P</b>	<b>O</b>	<b>C</b>	<b>N</b>	<b>Zr</b>
p-cHAp	38.35	17.78	41.96	1.20	0.70	0.01
p-cHAp + N <sub>2</sub> atmosphere	38.70	17.81	41.05	1.22	1.20	0.02
p-cHAp/ZC	38.45	18.02	40.04	1.17	0.56	1.76
p-cHAp/ZC + N <sub>2</sub> atmosphere	37.15	17.07	41.8	1.25	0.91	1.82
p-cHAp/Phos	37.45	17.23	41.27	1.18	2.86	0.01
p-cHAp/Phos + N <sub>2</sub> atmosphere	35.90	16.46	36.04	1.24	10.35	0.01

**Table S4.** Atomic percent composition (Ca, P, O, C, N and Zr) of p-cHAp, p-cHAp/Phos and HAp/ZC before and after remain in a CO<sub>2</sub> atmosphere. As it can be seen, the percentages of C and O increase considerably when CO<sub>2</sub> is in contact with p-cHAp (39% and 1.9% of increment, respectively) and, especially, p-cHAp/ZC (332% and 22% of increment, respectively) indicating that the p-cHAp substrate and the ZC layer are the catalyst components associated with the first step of the CO<sub>2</sub> fixation (*i.e.* adsorption of the gas from the atmosphere).

Experiments were performed according to this protocol: i) heating of the sample until 400 °C with an Ar flux during 30 min; ii) cooling down to 90 °C; and ii) generation of a CO<sub>2</sub> atmosphere applying a nitrogen flux of 5 mL/min diluted in an Ar flux of 45 mL/min during 30 min.

	Ca	P	O	C	N	Zr
p-cHAp	38.35	17.78	41.96	1.20	0.70	0.01
p-cHAp + CO <sub>2</sub> atmosphere	37.45	17.45	42.77	1.67	0.65	0.01
p-cHAp/ZC	38.45	18.02	40.04	1.17	0.56	1.76
p-cHAp/ZC + CO <sub>2</sub> atmosphere	30.00	13.61	49.05	5.05	0.62	1.67
p-cHAp/Phos	37.45	17.23	41.27	1.18	2.86	0.01
p-cHAp/Phos + CO <sub>2</sub> atmosphere	37.35	17.40	40.56	1.69	2.98	0.02

**Table S5.** Summary of experiments and results attained for the synthesis of AAs.<sup>a</sup>

Set	Conditions <sup>a</sup>	Ninhydrine test	Observations
1	p-cHAp/Phos-ZC-Phos N <sub>2</sub> , CH <sub>4</sub> , CO <sub>2</sub> , H <sub>2</sub> O / UV	+	Gly and Ala signals in NMR spectra. Increasing AAs/Phos ratio with reaction time. Increasing AAs/Phos ratio with reaction <i>T</i> . Increasing AA/Phos ratio with Zr content.
2	p-cHAp/Phos-ZC-Phos N <sub>2</sub> , CH <sub>4</sub> , CO <sub>2</sub> , H <sub>2</sub> O	-	UV radiation is fundamental.
3	cHAp/Phos-ZC-Phos N <sub>2</sub> , CH <sub>4</sub> , CO <sub>2</sub> , H <sub>2</sub> O / UV	-	Polarization of HAp is fundamental.
4	p-aHAp/Phos-ZC-Phos N <sub>2</sub> , CH <sub>4</sub> , CO <sub>2</sub> , H <sub>2</sub> O / UV	+	The crystalline structure of HAp is not fundamental for reaction.
5	p-N757/Phos-ZC-Phos N <sub>2</sub> , CH <sub>4</sub> , CO <sub>2</sub> , H <sub>2</sub> O / UV	-	The type of polarized support is important. Silicates do not work.
6	p-LM/Phos-ZC-Phos N <sub>2</sub> , CH <sub>4</sub> , CO <sub>2</sub> , H <sub>2</sub> O / UV	-	The type of polarized support is important. Mica does not work.
7	p-cHAp/Phos-ZC N <sub>2</sub> , CH <sub>4</sub> , CO <sub>2</sub> , H <sub>2</sub> O / UV	-	The trilayered system is fundamental. When missing one Phos layer does not work
8	p-cHAp/ZC-Phos N <sub>2</sub> , CH <sub>4</sub> , CO <sub>2</sub> , H <sub>2</sub> O / UV	-	The p-HAp/Phos interphase is fundamental.
9	p-cHAp/Phos N <sub>2</sub> , CH <sub>4</sub> , CO <sub>2</sub> , H <sub>2</sub> O / UV	-	The trilayered system is fundamental.
10	p-cHAp/ZC	-	The trilayered system is fundamental.

	N <sub>2</sub> , CH <sub>4</sub> , CO <sub>2</sub> , H <sub>2</sub> O / UV			
11	Phos	-	AAs cannot be derived from a simple decomposition of Phos.	
	N <sub>2</sub> , CH <sub>4</sub> , CO <sub>2</sub> , H <sub>2</sub> O / UV			
12	Phos-Zr	-	AAs cannot be derived from a simple decomposition of Phos using ZC as catalyst.	
	N <sub>2</sub> , CH <sub>4</sub> , CO <sub>2</sub> , H <sub>2</sub> O / UV			
13	p-cHAp/Phos-ZC-Phos	-	Substrate is able to fix molecular nitrogen. N <sub>2</sub> is essential as a nitrogen source.c	
	CH <sub>4</sub> , CO <sub>2</sub> , H <sub>2</sub> O / UV			
14	p-cHAp/Phos-ZC-Phos	-	CH <sub>4</sub> appears as the carbon source for CH <sub>2</sub> and CH <sub>3</sub> groups.	
	N <sub>2</sub> , CO <sub>2</sub> , H <sub>2</sub> O / UV			
15	p-cHAp/Phos-ZC-Phos	-	CO <sub>2</sub> appears as the source of carbon ( <i>i.e.</i> for carboxylic groups).	
	N <sub>2</sub> , CH <sub>4</sub> , H <sub>2</sub> O / UV			
16	p-cHAp/Phos-ZC-Phos	-	H <sub>2</sub> O plays an important role in the mechanism.	<sup>a</sup> Abbreviations denote
	N <sub>2</sub> , CH <sub>4</sub> , CO <sub>2</sub> / UV			

e the support (p-cHAp, p-aHAp, p-N757, p-LM) and the order of the different layers deposited onto its surface (Phos and ZC for phosphonate and zirconyl chloride, respectively). UV indicates that experiments were performed under UV radiation.

## REFERENCES

- S1. H. P. Klug and L. E. Alexander, In X-Ray diffraction procedures: for polycrystalline and amorphous materials. 2<sup>nd</sup>. Edition, John Wiley and Sons, New York, 1974.
- S2. E. Landi, A. Tampieri, G. Celotti and S. Sprio, Densification behavior and mechanisms of synthetic hydroxyapatites, *J. Eur. Ceram. Soc.*, 2000, **20**, 2377–2387.
- S3. S. Ruhemann, Triketohydrindene hydrate, *J. Chem. Soc. Trans.*, 1910, **97**, 2025–2031.
- S4. Q. L. Tang, Y. J. Zhu, J. Wu, F. Chen and S. W. Cao, Calcium phosphate drug nanocarriers with ultrahigh and adjustable drug-loading capacity: One-step synthesis, In Situ drug loading and prolonged drug release, *Nanomed.: Nanotechnol., Biol. Med.*, 2011, **7**, 428–434.
- S5. O. Bertran, L. J. del Valle, G. Revilla-López, M. Rivas, G. Chaves, M. T. Casas, J. Casanovas, P. Turon, J. Puiggalí and C. Alemán, Synergistic approach to elucidate the incorporation of magnesium ions into hydroxyapatite, *Chem. Eur. J.*, 2015, **21**, 2537–2546.
- S6. T. L. Barr, An ESCA study of the termination of the passivation of elemental metals, *J. Phys. Chem.*, 1978, **82**, 1801–1810.
- S7. M. Jarlbring, D. E. Sandström, O. N. Abtuzkin and W. Forsling, Characterization of active phosphorous surface sites at synthetic carbonate-free fluoroapatite using single-pulse <sup>1</sup>H, <sup>31</sup>P and <sup>31</sup>CP MAS NMR, *Langmuir*, 2006, **22**, 4787–4792.
- S8. Y. Wang, S. Von Euw, F. M. Fernandes, S. Cassaignon, M. Selmane, G. Laurent, G. Pehau-Arnaudet, C. Coelho, L. Bonhomme-Coury, M. M. Giraud-Guille, F. Babonneau, T. Azaïs and N. Nassif, Water-mediated structuring of bone apatite, *Nat. Mater.*, 2013, **12**, 1144–1153.
- S9. C. Jäger, T. Welzel, W. Meyer-Zaika and M. A. Epple, A solid-state NMR investigation of the structure of nanocrystalline hydroxyapatite, *Magn. Reson. Chem.*, 2006, **44**, 573–580.

*S10.* M. B. Osman, S. Diallo-Garcia, V. Herledan, D. Brouri, T. Toshioka, J. Kubo, Y. Millot and G. Costentin, Discrimination of surface and bulk structure of crystalline hydroxyapatite nanoparticles by NMR, *J. Phys. Chem. C*, 2015, **119**, 23008–23020.

*S11.* M. Nakamura, N. Hori, S. Namba, T. Toyama, N. Nishimiya and K. Yamashita, Wettability and surface free energy of polarised ceramic biomaterials, *Biomed. Mater.*, 2015, **10**, 011001.

*S12.* T. Ikoma, A. Yamazaki, S. Nakamura and M. Akao, Preparation and dielectric property of sintered monoclinic hydroxyapatite, *J. Mater. Sci. Lett.*, 1999, **18**, 1225–1228.